nature ecology & evolution

SUPPLEMENTARY INFORMATION

https://doi.org/10.1038/s41559-019-0904-4

In the format provided by the authors and unedited.

Three thousand years of wild capuchin stone tool use

Tiago Falótico[1,2,6], Tomos Proffitt[3,6*], Eduardo B. Ottoni[1], Richard A. Staff[4] and Michael Haslam[5]

[1]Department of Experimental Psychology, Institute of Psychology, University of São Paulo, Butantã, Brazil. [2]Neotropical Primates Research Group, Butantã, Brazil. [3]Institute of Archaeology, University College London, London, UK. [4]Scottish Universities Environmental Research Centre, East Kilbride, UK. [5]Independent Researcher, London, UK. [6]These authors contributed equally: T. Falótico, T. Proffitt. *e-mail: t.proffitt@ucl.ac.uk

Supplementary Online Material - 3000 years of wild capuchin stone tool use

Authors: Tiago Falótico[1,2] †, Tomos Proffitt[3]*†, Eduardo B. Ottoni[1], Richard A. Staff[4], Michael Haslam[5]

Correspondence to: t.proffitt@ucl.ac.uk

1. Supplementary Information - Lithic analysis

1.1. Artefact frequencies

Quartzite is the most prevalent raw material in every chronological phase at Caju BPF2 (n = 101, 97.1%). This raw material is abundant throughout Serra da Capivara National Park. A far smaller number of artefacts in the upper chronological phases (Phases I and II) are produced on sandstone (n = 3, 2.9%), which is, overall, more scarce within the landscape.

A total of 46.7kg of lithic material recovered from Caju BPF2 exhibits evidence of percussive damage and can be considered utilised. Using the Wentworth scale[1] of clast dimensions the lithic material is dominated by artefacts produced on pebbles (n = 85, 81.7%) with a smaller percentage produced on larger cobbles (n = 19, 18.3%).

The Caju BPF2 excavation yielded a total of 122 capuchin modified lithic artefacts. Active percussive tools predominate (hammerstones, broken hammerstones, hammerstones with flake detachments), with a far smaller percentage of passive elements (anvils) and fragments (anvil fragments, chunks, percussive flakes) (Supplementary Table 2).

Diachronic artefact composition varied between the stratigraphic phases, with a Chi-square test indicating a significant difference in tool categories between phases ($X^2(15) = 58.562$, $p = 0.000$) (Cramer's V Value 0.0.433, $p = 0.000$). Post hoc analysis indicates that this variation is a result of an abundance of complete hammerstones in Phase I, an over-representation of anvils and fragments and an under-representation of complete and flaked hammerstones in Phase II, and an over-representation of flaked hammerstones and an under-representation of anvils, and fragments in Phase IV, whilst Phase III shows no variation.

1.2. Hammerstones

Hammerstones are the most prevalent artefact at Caju BPF2, and can be divided into three sub-categories: complete hammerstones, broken hammerstones, and hammerstones with flake detachments. Of these, complete hammerstones are the most frequent (n = 75, 61.5%), with hammerstones with flake detachments (n = 14, 11.5%) and broken hammerstones (n = 8, 6.6%) making up far smaller percentages of the entire assemblage (Supplementary Figure 1).

When considering all hammerstones, there is a difference in colouration between phases. All hammerstones from Phase I possess visually identifiable residue, giving them a darker brown / yellow colour, compared to the brighter coloured hammerstones identified in the older phases (Phases II, III and IV) (Supplementary Figure 3). This colouration is in keeping with typical cashew residue. Two possibilities can explain this difference in colouration. The most parsimonious explanation is varying levels of preservation of cashew nut oil on the surface of the hammerstones. However, the lack of cashew nut residue on hammerstones from Phases II, III and IV may also be associated with variation of hammerstone use by capuchins over time.

There is a significant difference in the frequency of hammerstone categories between chronological phases (Cramer's V (X^2 = 0.388, p = <0.001). Post hoc analysis indicates that hammerstones with flake removals are over-represented in Phase IV, and broken hammerstones are over-represented in Phase II (Supplementary Figure 3).

1.3. Complete hammerstones and hammerstones with flake detachments

Complete hammerstones possess a mean length, width and thickness of 64.4 x 48.5 x 35.5mm, and weigh on average 152.8g (Supplementary Table 3). Comparing hammerstone dimensions and weight during each chronological phase to the natural sample of cobbles reveals a significant difference in all dimensions and weight. This trend is also clear when all complete hammerstones and flaked hammerstones are compared by chronological phase to the natural sample of cobbles. The data therefore demonstrate that capuchins were consistently selecting larger hammerstones from the surrounding landscape, during each phase of occupation.

As there is no significant difference in the dimensions and weight of complete hammerstones and hammerstones with flake detachments (see below), they are considered together when assessing diachronic variation in metrics. A Kruscal-Wallis Test indicates that there is a significant difference in all dimensions (length (X^2 (3) = 10.758, p = 0.013), width (X^2 (3) = 13.269, p = 0.004), thickness (X^2 (3) = 11.69, p = 0.009) and weight (X^2 (3) = 15.007, p = 0.002)) (Supplementary Figure 2), of complete and flake detachment hammerstones between chronological phases. Post hoc analysis indicates that this difference is based on differences between hammerstones in Phase IV and Phase II, with those from Phase II being significantly larger and heavier (Mann-Whitney U: Length: U = 20, p = 0.004; Width: U = 18, p = 0.003; Thickness: U = 12, p = 0.001; Weight: U = 12, p = 0.001). Furthermore, a Mann-Whitney U test shows that hammerstones in Phase II are significantly longer (U = 156, p = 0.042), thicker (U = 172, p = 0.007) and heavier (U = 163, p = 0.020) than those in Phase I. There is no significant difference between the hammerstones found in Phase III and the other phases.

The capuchins used cobbles (n = 41, 71.9%) for the majority of complete hammerstones, however, a small number of broken cobbles (n = 16, 28.1%) were also used. These cobbles were broken during prior geological time periods and are not fragmented as a consequence of capuchin percussive action, as demonstrated by their heavily weathered margins and lack of recent fragmentation. The majority of these hammerstones are either plano-convex (n = 23, 40.4%), or tabular (n = 20, 35.1%) in morphology. A small number of irregular (n = 11, 19.3%), bi-convex (n = 2, 3.5%) and plano-convex (n = 1, 1.8%) cobbles are also present. A chi-square (Cramer's V) test indicates that there is no significant difference in blank morphology between chronological phases ($X^2 = 0.229$, $p = 0.707$). When compared to a sample of 1315 natural cobbles selected from the surrounding area, a chi-square test on cobble morphology indicates a significant difference (Cramer's V) ($X^2 = 0.097$, $p = 0.025$) between the Caju BPF2 artefacts and the morphology of the natural cobbles. Post hoc analysis indicates a significant over-representation of plano-convex cobbles used as hammerstones, along with a significant under-representation of irregular cobbles. This finding suggests that capuchins were actively selecting specific cobble shapes to use as hammerstones, and actively avoiding irregular cobbles and those with concave surfaces.

When all complete hammerstones are assessed in terms of geological particle shape (Sneed and Folk Classifications)[2], compact-elongated cobbles are most prevalent (n = 14, 24.6%), followed by compact-bladed (n = 12, 21.1%). An equal frequency of bladed (n = 8, 14%), compact (n = 8, 14%) and compact-platy (n = 8, 14%) are also represented, along with a far smaller percentage of elongated (n = 5, 8.8%) and platy (n = 2, 3.5%) cobbles. Compared to the make-up of natural unmodified cobbles, a chi-square test (Cramer's V) indicates no significant difference ($X^2 = 0.110$, $p = 0.058$), however a post hoc analysis indicates that there is a significant over-representation of compact-elongated blanks used as hammerstones, and a significant under-representation of bladed blanks.

Percussive damage on complete hammerstones is characterised by the presence of multiple individual incipient cones of percussion (n = 36, 63.2%), the adherence of residue (n = 18, 31.6%), crushing of the surface of the hammerstone (n = 1, 1.8%), or a combination of these (n = 2, 3.6%). Impact points and crushing are the only two types that can be considered as permanent percussive damage (Supplementary Figure 3). The majority of complete hammerstones possess between 5 and 20 impacts (n = 27, 69.2%), with only three examples possessing in excess of 20 separate impact points. A chi-square test (Cramer's V) indicates that there is a significant chronological variation in the frequency of impact points on complete hammerstones ($X^2 = 0.588$, $p = 0.000$). Post hoc analysis indicates that this variation is due to an over-representation of hammerstones with no impact points in Phase I, and over-representation of between 1 and 5 impacts in Phase II, along with an over-representation of 6-10 and 11-15 impacts in phase IV. The increased prevalence of highly damaged hammerstones in the older phases is also clear, with the only examples of complete hammerstones with >20 impacts coming from Phases III and IV (Supplementary Figure 4).

Residue adhering to hammerstones largely covers all surfaces due to its viscous nature, and as such provides little information regarding the manual handling of hammerstones. Once hammerstones exclusively covered in residue are removed from the sample, percussive damage in the form of impact points and crushing is primarily located on 1 (n = 12, 30.8%) or 2 (n = 15, 38.5%) surfaces, with much less damage located on 3 or more surfaces (n = 12, 30.8%). There is no significant difference between chronological phases in the number of surfaces that possess percussive damage (Cramer's V) (χ^2 = 0.234, p = 0.896).

Percussive damage is either exclusively located on flat surfaces (n = 12, 30.8%), or less often in combination with damage along intersecting edges (n = 9, 23.1%), with convex surfaces (n = 5, 12.8%), or both (n = 2, 5.1%). To a far lesser extent, damage is located exclusively along intersecting edges (n = 5, 12.8%) or on convex surfaces (n = 3, 7.7%) or a combination of both (n = 3, 7.7%). There is no significant difference in the morphological location of percussive damage between the various chronological phases of the site. However, there is an increase in the range of morphological locations of percussive damage in Phases III and IV, compared to Phases I and II (Supplementary Figure 5). These patterns suggest that hammerstones were more frequently rotated during use in Phases III and IV, or that the target object was smaller or harder resulting in increased mis-hits.

1.4. Hammerstones with flake detachments

Hammerstones with flake detachments have an unintentional detachment of one or more flakes owing to repeated percussive action. These tools are exclusively associated with the earlier chronological phases (III and IV), with all but one found in Phase IV (n = 12, 92.3%). On average, they measure 60.6 x 46.3 x 35.4 mm and weigh 154.7 g (Supplementary Table 3). There is no significant difference in dimensions between complete hammerstones and hammerstones with flake removals (Mann-Whitney U: length (U = 394.5, p = 0.274); width (U = 380, p = 0.206); thickness (U = 438, p = 0.560; weight (U = 382.5, p = 0.217)). Tabular blanks are the most frequent morphology for this artefact type (n = 6, 46.2%), however, plano-convex (n = 3, 23.1%), bi-convex (n = 2, 15.4%) and irregular blanks (n = 2, 15.4%) are also represented. The percussive damage associated with hammerstones with flake detachments consists of repeated individual impacts as well as a small degree of crushing of the surface of the hammerstone. There is no significant difference between flaked hammerstones and complete hammerstones in the number of planes that exhibit percussive damage. The majority of flaked hammerstones possess damage on three or more separate planes. However, the frequency of impact points on flaked hammerstones is significantly greater than that identified on complete hammerstones (Chi-square Cramer's V) X^2 = 0.562, p = 0.012) (Supplementary Figure 6), indicating a far higher degree of percussive action on hammerstones that have one or more unintentional flake detachments.

The number of flake detachments varies between 1 and 3; however, the majority (n = 7, 53.9%) possess two or three removals. On average, these removals are small (19.3 mm x 18 mm) and non-invasive. In each case, the flake removals are wedge initiated from flat or convex surfaces and can be considered equivalent, in terms of fracture mechanics, to that of a typical knapping hammerstone flake detachment. In no instance was a flake detached from an angle of less than 90 degrees and none can be considered as conchoidal removals (Supplementary Figure 7).

1.5. Broken hammerstones

Broken hammerstones make up a small proportion of the entire lithic assemblage. On average they measure 65.7 x 48.6 x 35.3 mm and weigh 156.3 g (Supplementary Table 3). The majority possess a plano-convex (n = 4, 50%) morphology, with smaller frequencies of tabular (n = 3, 37.5%) and irregular (n = 1, 12.5%) morphologies also present. All broken hammerstones present the same breakage pattern, with a single transverse fracture caused by either a single or a small number of impacts towards the center of the hammerstone. The percussive damage is similar to that seen on complete hammerstones, characterised by individual incipient cones of percussion (n = 6, 75%), or a combination of individual impacts and crushing of the quartz crystals (n = 2, 25%). In no case is there evidence of percussive damage located on the newly fractured plane, suggesting that either these hammerstones saw little rotation during use, or were discarded once broken. There is no significant diachronic variation in percussive damage intensity for broken hammerstones.

1.6. Anvils

The majority of anvils are large quartzite cobbles (n = 11, 78.6%), measuring on average 165.1 x 123.8 x 92 mm and weighing 2510.6 g (Supplementary Table 3). However, a few (n = 3, 21.4%) smaller sandstone anvils are also present, measuring on average 115.1 x 91 x 59.4 mm and weighing 1157.1 g.

Anvils are distinct from hammerstones in terms of both dimensions and degree of percussive damage. A Mann-Whitney U test shows that anvils are significantly larger in every dimension (length (U = 16, p = <0.001), width (U = 29, p = <0.001), and thickness (U = 67, p = <0.001)) as well as being heavier than all hammerstones (U = 22, p = <0.001) (Supplementary Figure 8).

Percussive damage on anvils is primarily located across topographically raised convex regions. The degree of percussive damage is high, with quartzite anvils characterised by frequent overlapping incipient cones of percussion, often across the entire surface of the anvil. Sandstone anvils, however, develop a high degree of crushing of the surface across topological high regions. A small number (n = 5, 35.7%) of anvils possess significant fractures along a single edge caused by repeated percussive impacts (Supplementary Figure 9).

1.7. Fragments

Fragmented pieces comprise only a small percentage of the total lithic assemblage (n = 10, 9.26%), and consist primarily of anvil fragments (n = 8, 88.9%) as well as an individual angular chunk (11.1%). All anvil fragments share similar taphanomic and technological characteristics. The majority of anvil fragments are found within Phase II, specifically within the same excavation level (Level 3) as the majority of the anvils.

The percussive damage on anvil fragments is characterised by one or more large percussive impacts (incipient cones of percussion) located along a fracture margin or edge. The substantial nature and location of these impacts suggests that they were the initial cause of the anvil fragmentation, however, the fracturing occurred along pre-existing internal fracture planes. The location of the initiating impact points suggests that these anvil fragments were detached from close to the edge of the anvil.

The passive origin of these artefacts can be inferred from the substantial percussive impacts located on their cortical surfaces, located along fracture planes, as well as their significantly greater dimensions (Mann-Whitney U: length (U = 0.000, $p = 0.000$), width (U = 2, $p = 0.000$)) than any flake removals identified on flaked hammerstones (Supplementary Figure 10).

1.8. Percussive flakes

Two (1.9%) fragmented pieces can be considered percussive flakes (Supplementary Figure 11). Both flakes are wedge initiated and possess fully cortical convex platforms. One flake possesses a fully cortical dorsal surface with a small number of incipient cones of percussion, suggesting a degree of rotation during the percussive behaviour. The second flake shows evidence of a single previous detachment on the dorsal surface, which is <50% cortical.

Although considerably smaller than the average hammerstone flake detachment, the smaller of the two percussive removals fits morphologically within this category (Supplementary Figure 12). However, the second percussive removal more closely resembles, morphologically, a detachment from the edge of an anvil. In each case the initiation was a forceful wedge. There is a clear disparity between the number of wedge initiated percussive flake removals (n = 22) identified on the flaked hammerstones and the total number of recovered percussive flakes from the excavated sample (n = 2). This may be due to the conservative manner in which artefacts were differentiated from natural unmodified lithics.

2. Radiocarbon dating

Radiocarbon (^{14}C) dating of the Caju BPF2 stratigraphic sequence builds upon that presented by Haslam et al.[7]. In total, fifteen charcoal samples were selected for ^{14}C dating at the Oxford Radiocarbon Accelerator Unit (ORAU, University of Oxford, UK). Of these samples, two were from Phase II, five from Phase III, and eight from Phase IV (the oldest unit with associated capuchin stone tools) (Supplementary Tabl 1) (Supplementary Figure 13 A and B).

Prior to sub-sampling, the surface of each charcoal sample was physically cleaned (with a clean scalpel blade). A minimum of 35 mg of clean, black charcoal was taken for each sub-sample. Two sub-samples were taken from one of the samples (FUMDHAM no. 221934), to produce replicate ^{14}C measurements (part of ORAU's internal laboratory quality assurance protocol)[3].

A chemical pre-treatment for ^{14}C dating was subsequently applied, following the routine acid-base-acid (ABA) protocol of Brock et al[3]. Briefly, this involved successive 1 M HCl (20 mins, 80 °C), 0.2 M NaOH (20 mins, 80 °C) and 1 M HCl (1 hr, 80 °C) washes, with each stage followed by rinsing (≥3 times) with ultrapure MilliQ™ deionised water. The three main stages of this process are similar across most radiocarbon laboratories and are respectively intended to remove: (i) sedimentary- and other carbonate contamination; (ii) organic (principally humic- and fulvic-) acid contamination; and (iii) any dissolved atmospheric CO_2 that might have been introduced during the preceding base wash. In this way, any potential secondary carbon contaminants are removed, leaving the samples pure for subsequent combustion on an elemental analyser (EA), coupled to an isotope ratio mass spectrometer (IRMS) and a bespoke cryogenic CO_2 collection system. All samples gave good (>50% C) combustion yields, and stable carbon isotope ratios ($\delta^{13}C$) of between -26.6 and -22.9‰ (Supplementary Table 1). Samples were subsequently graphitised (for 6 hours at 560ºC) and pressed into aluminium targets for accelerator mass spectrometry (AMS) ^{14}C dating, which was performed using the 2.5 MV HVEE tandem AMS system at ORAU[4, 33].

Individual ^{14}C ages varied between 109 ± 21 ^{14}C years before present (BP) at the top of the dated sequence (Phase II), and 3698 ± 33 BP at the base (Phase IV). These ^{14}C data were subsequently analysed using the Bayesian statistical software OxCal ver. 4.3[6], applying the Southern Hemisphere 'SHCal13'[7] and 'Bomb13SH3'[8] calibration curves. The data were grouped into four successive 'Phases' (I to IV) constrained within a 'Sequence' deposition model[9], specifying only that these four Phases followed the law of stratigraphic superposition (i.e. that shallower depositional units must post-date underlying sedimentological units), but making no assumption within each model Phase (depositional unit) as to the relative ordering of samples. In contrast to lacustrine or marine sediment profiles that might exhibit more regular deposition[10], such Sequence and Phase models are the most suitable for sedimentological settings such as at Caju BPF2, where the continuity of deposition is unknown[11]. At the start and end of each of the four model Phases (i.e. the bottom and top of each of the four depositional units) model 'Boundaries' were inserted, and an additional constraining date of AD 2014 (i.e. the date of field sampling) was included at the top of the Sequence. Additionally, outlier analysis was applied to objectively identify and down-weight the influence of any spurious measurements using the 'General' 'Outlier_Model' described by Bronk Ramsey[12]. A prior 'Outlier' probability of 5% was applied to each of the ^{14}C determinations since there was no reason, a priori, to suggest that any of the samples were more likely to be statistically outlying than others. Finally, summary statistics (in the form of ‘Date’ functions) were included for each of the four Phases to describe the full time ranges represented by each of the depositional units themselves.

The output of the model provides age ranges for: the uppermost depositional unit (Phase I) of 1973 to 2014 cal AD (68.2% highest probability density range, i.e. approximately equivalent to a 1 standard deviation range), 1890 to 2014 cal AD (95.4% highest probability density range, i.e. approximately equivalent to a 2 standard deviation range); for Phase II, 1693 to 1924 cal AD (68.2% range), 1614 to 1958 cal AD (95.4% range); for Phase III, 1310 to 1385 cal AD (68.2% range), 1265 to 1423 cal AD (95.4% range); and for the lowest of the excavated depositional units (Phase IV), 1044 to 473 cal BC (68.2% range), 1269 to 214 cal BC (95.4% range) (Supplementary Figure S14). The span of Phase IV (830 years, 68.2% range; 1055 years, 95.4% range), the lowermost to include associated capuchin archaeology, exhibits a more lengthy accumulation period than the overlying Phase III, for example, for which capuchin-worked stone tools have previously been reported. A single radiocarbon determination, that of OxA-33133 (FUMDHAM sample no. 226235), is the only sample flagged as being a likely statistical outlier (posterior outlier probability >50%) and therefore this sample was excluded from the final age-depth model (the age ranges for which having been presented above, and in the main text). If instead this age were left in the model, the antiquity of Phase IV would be extended to 1202 to 354 cal BC (68.2% range), 2130 to 142 cal BC (95.4% range). However, because of the sensitivity of this latter model output to the inclusion of the single, older charcoal sample (objectively identified as having >50% probability of being a statistical outlier – i.e. more likely to be a statistical outlier than not), we prefer to exclude this sample for the presentation of our finalised conclusions. All remaining ^{14}C samples have posterior outlier probabilities of ≤4%, demonstrating the integrity of the stratigraphic sequence, and giving good confidence in the ages of the associated capuchin archaeology.

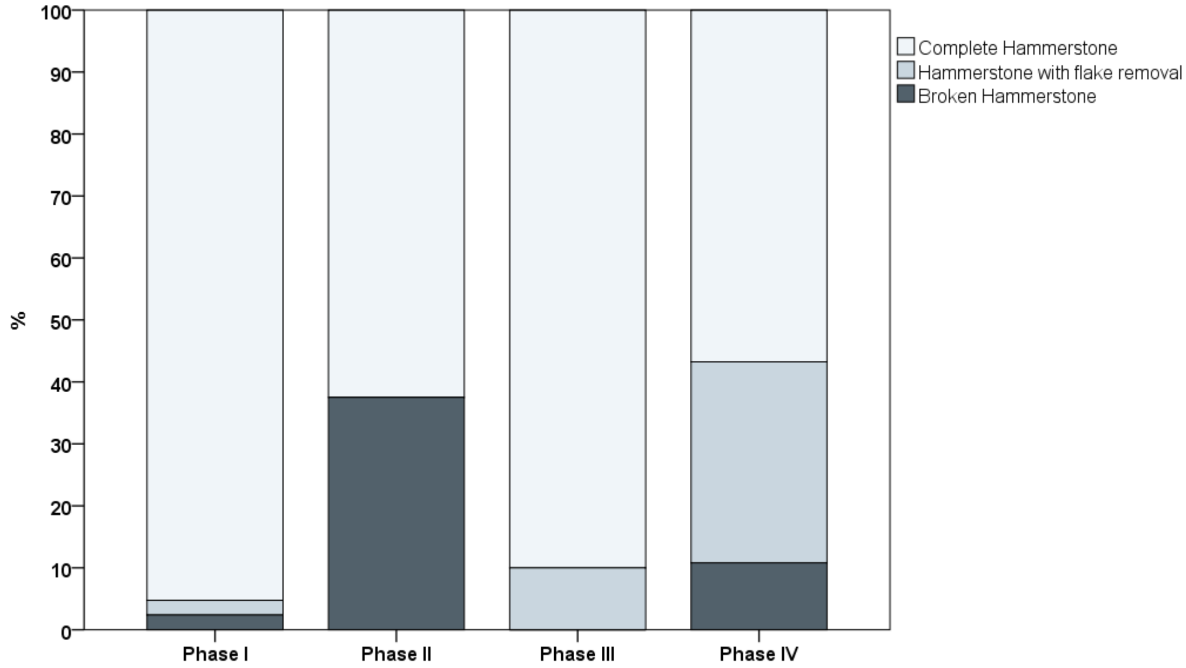

Supplementary Figure 1. *Absolute and relative frequencies of hammerstone categories separated by chronological phase at Caju BPF2.*

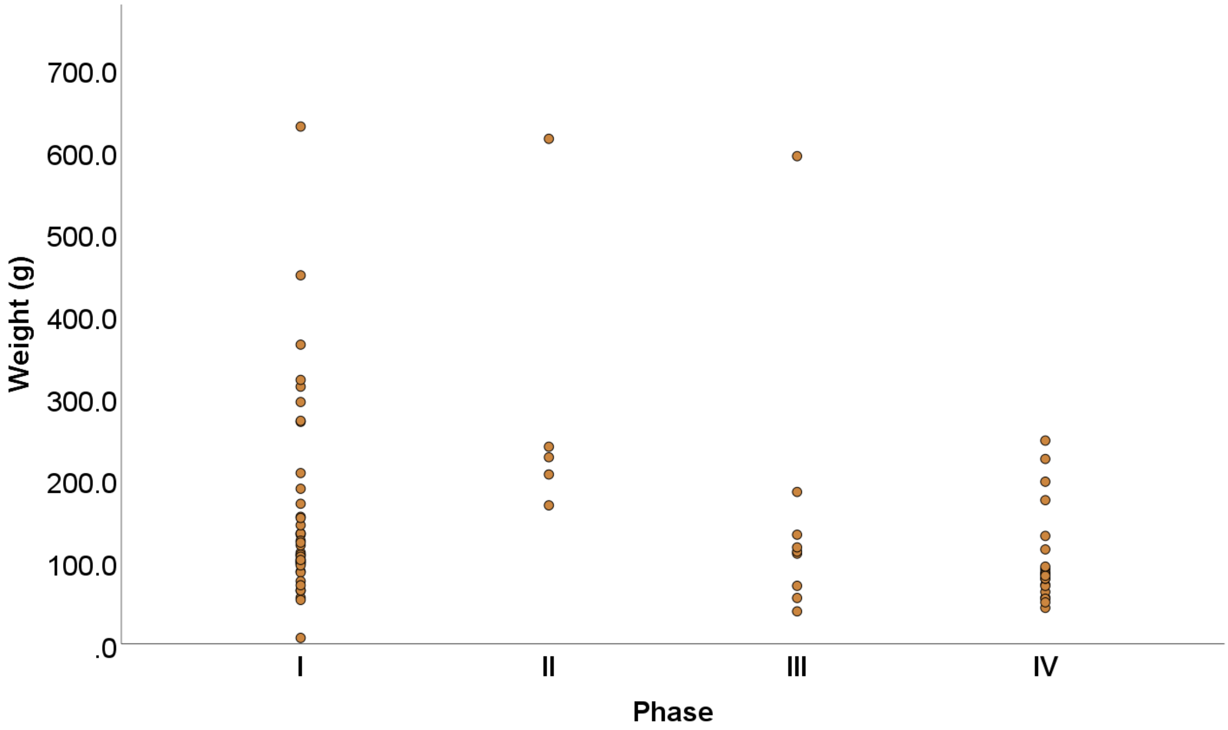

Supplementary Figure 2. *Weight (g) of all complete hammerstones at Caju BPF2, separated by chronological phases*

1

Supplementary Figure 3. *Examples of complete and fragmented capuchin hammerstones from Caju BPF2.* ***(A)*** *Broken hammerstone (#225888) from Phase II.* ***(B)*** *Complete hammerstone (#225456) from Phase III.* ***(C)*** *Complete hammerstones (#226374) from Phase IV.* ***(D)*** *Hammerstone with flake detachment (#226454) from Phase IV.* ***(E)*** *Complete hammerstone (#226492) from Phase IV.* ***(F)*** *Complete hammerstone (#226502) from Phase IV).*

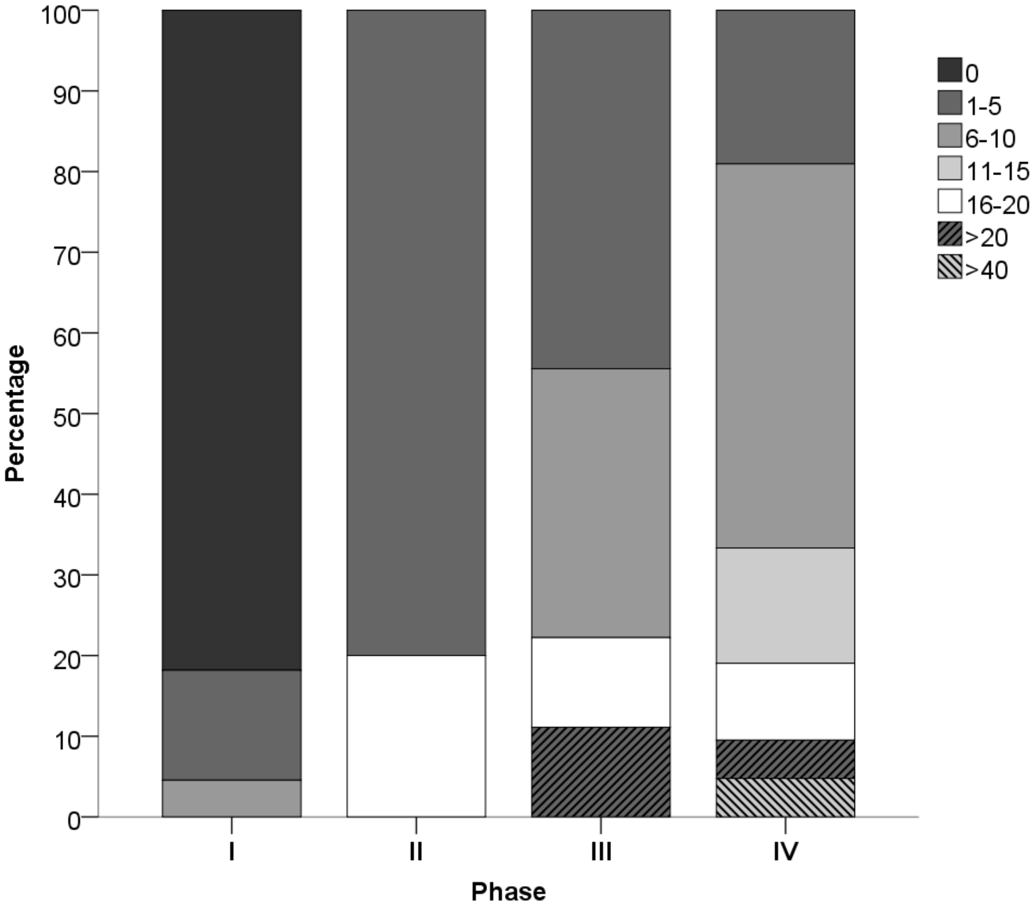

Supplementary Figure 4. *Relative frequencies of impact point ranges for all complete hammerstones at Caju BPF2, separated by chronological phase*

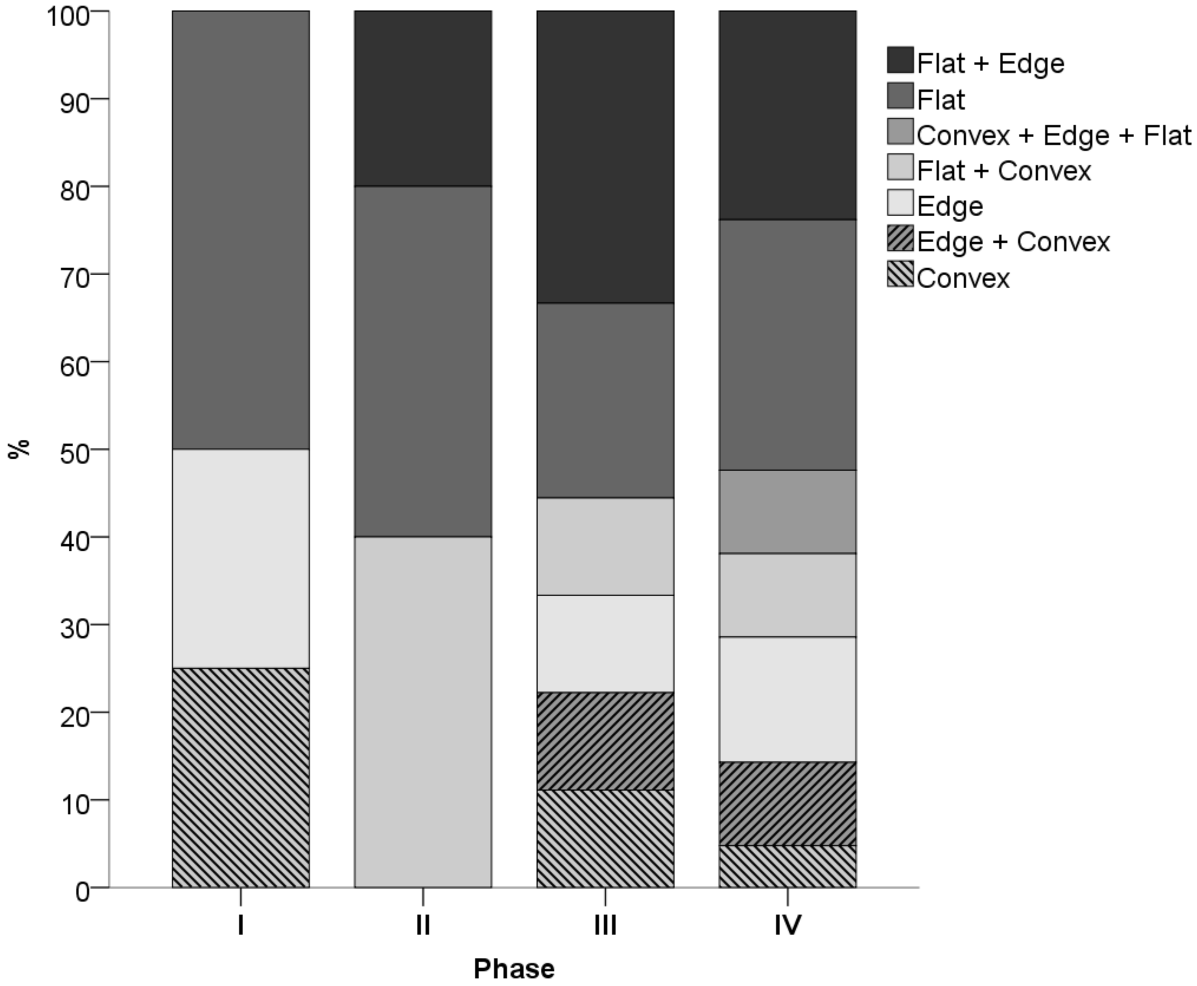

Supplementary Figure 5. *Relative frequencies of morphological locations of percussive damage on all non-residue- complete hammerstones at Caju BPF2*

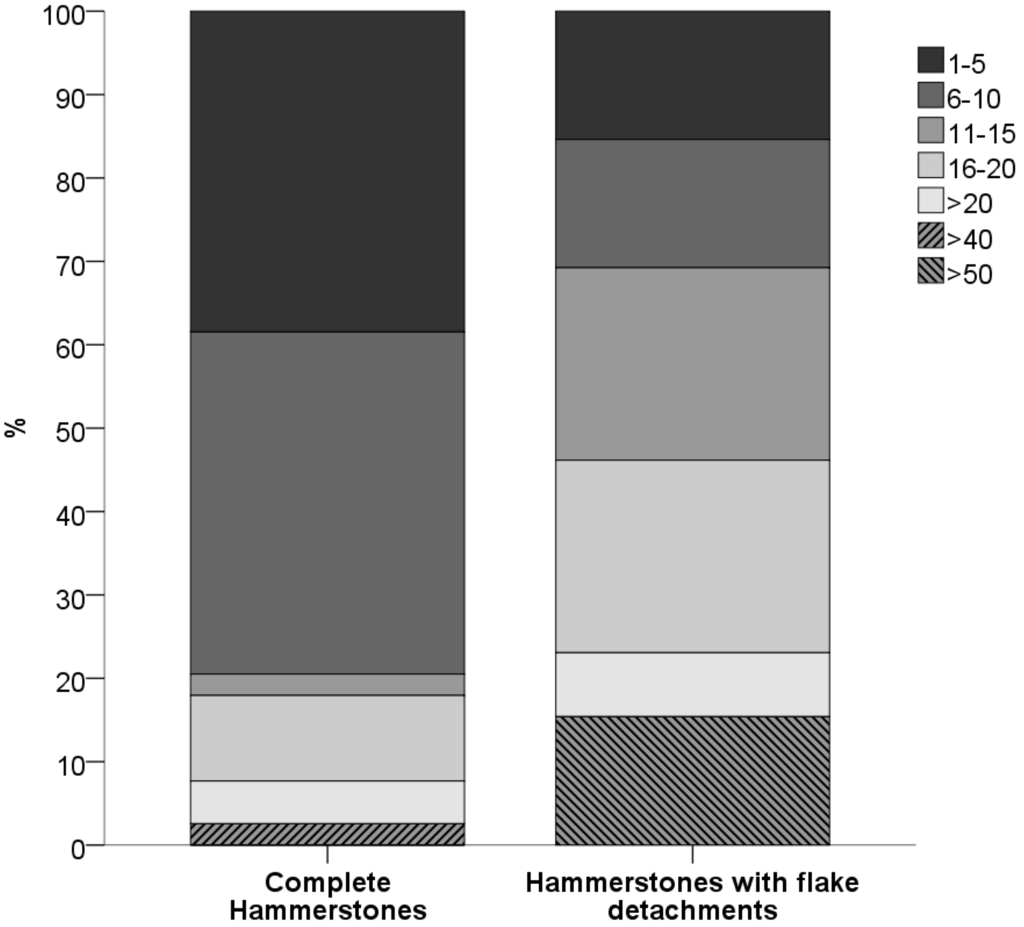

Supplementary Figure 6. *Relative frequencies of impact point ranges for all hammerstones with flake detachments and complete hammerstones at Caju BPF2*

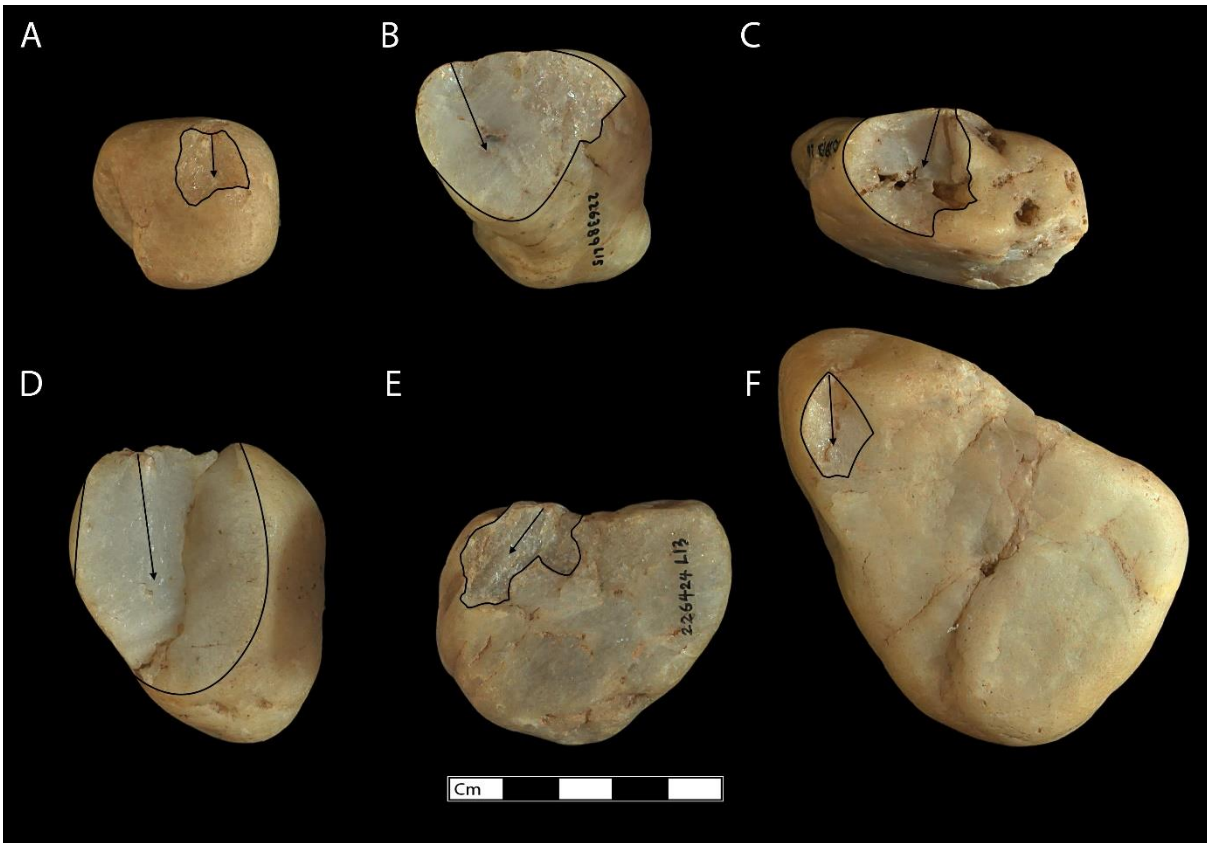

Supplementary Figure 7. *Examples of hammerstones with flake detachments from Caju BPF2.* ***(A)*** *#226353 from Phase IV.* ***(B)*** *#226389 from Phase IV.* ***(C)*** *#228388 from Phase IV.* ***(D)*** *#226477 from Phase IV.* ***(E)*** *#226424 from Phase IV.* ***(F)*** *#226360 from Phase IV.*

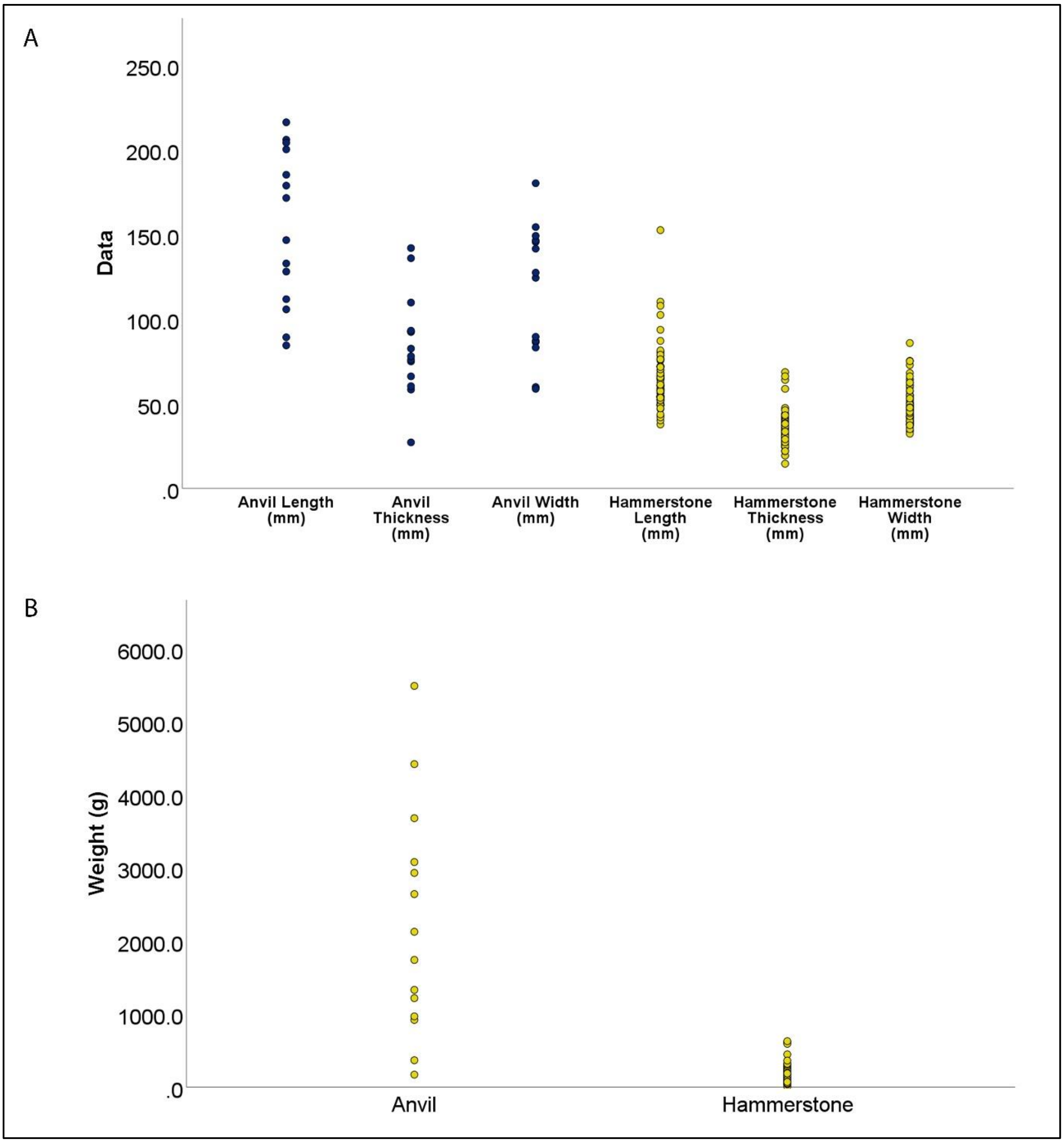

Supplementary Figure 8. *Comparisons of dimensions and weight of all anvils and complete hammerstones at Caju BPF2.* ***(A)*** *Length (mm), width (mm), and thickness (mm) comparisons of anvils and hammerstones.* ***(B)*** *Weight (g) comparisons of anvils and hammerstones*

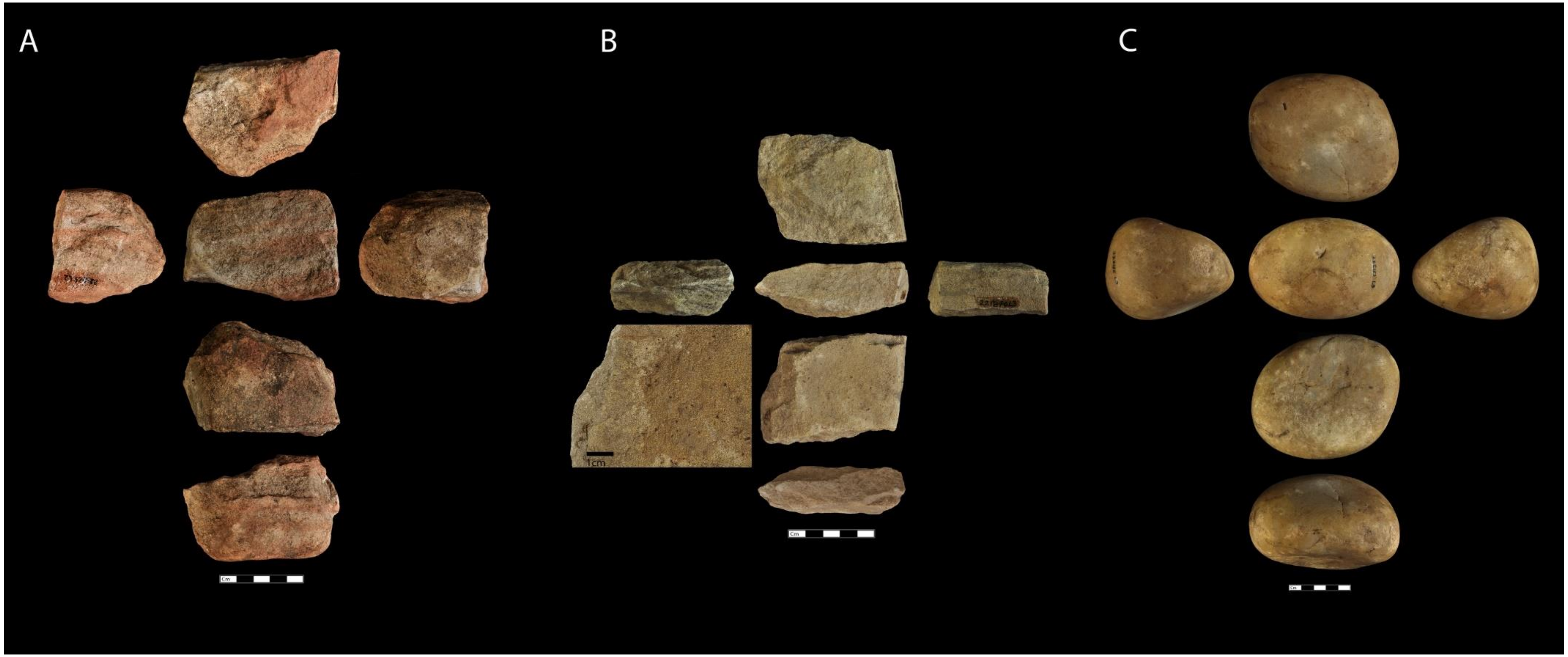

Supplementary Figure 9. *Examples of excavated capuchin anvils from Caju BPF2.* ***(A)*** *Anvil (#221825) from Phase I.* ***(B)*** *Anvil (#221870) from Phase III****. (C)*** *Anvil (#222153) from Phase III.*

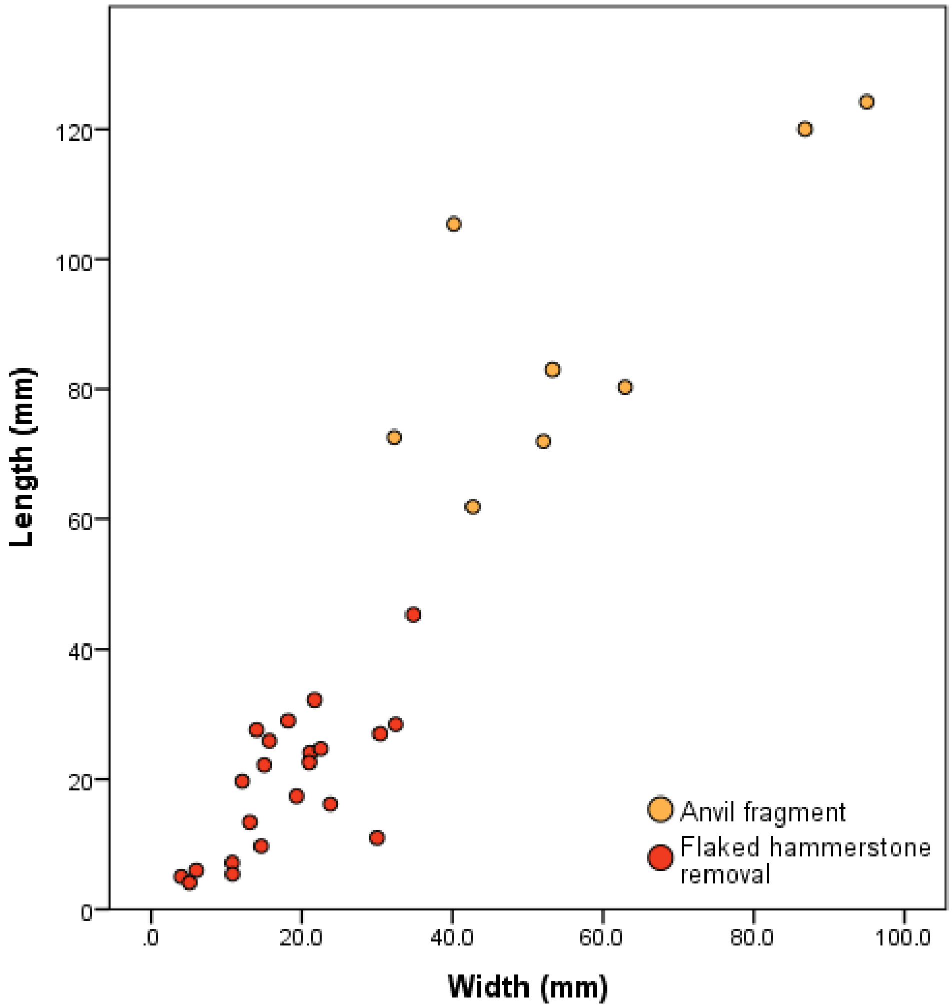

Supplementary Figure 10. *Maximum length (mm) and width (mm) of all flake scars on flaked hammerstones at Caju BPF2, compared to dimensions of anvil fragments*

Supplementary Figure 11. *Percussive flakes from Caju BPF2.* ***(A)*** *#222097 from Phase I.* ***(B)*** *# 226021 from Phase III.*

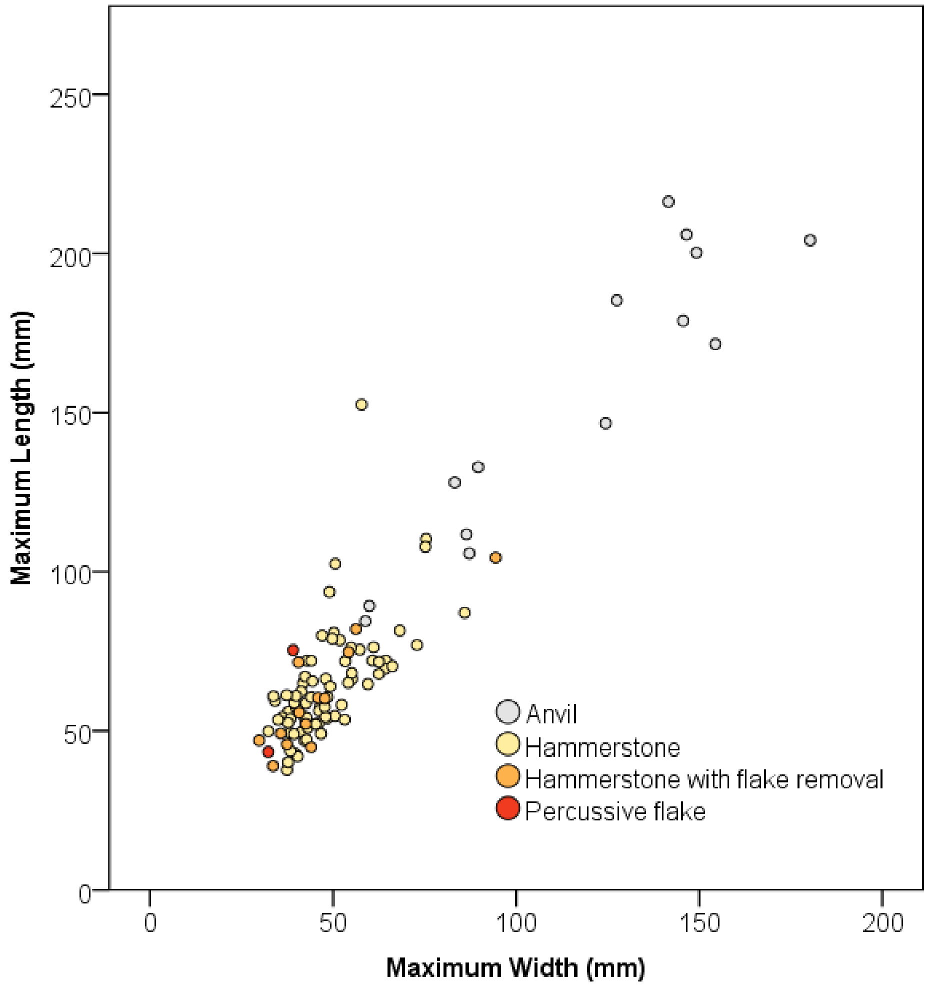

Supplementary 12. *Comparison of maximum length and width (mm) of percussive flakes, complete hammerstones, flaked hammerstones and anvils at Caju BPF2*

A

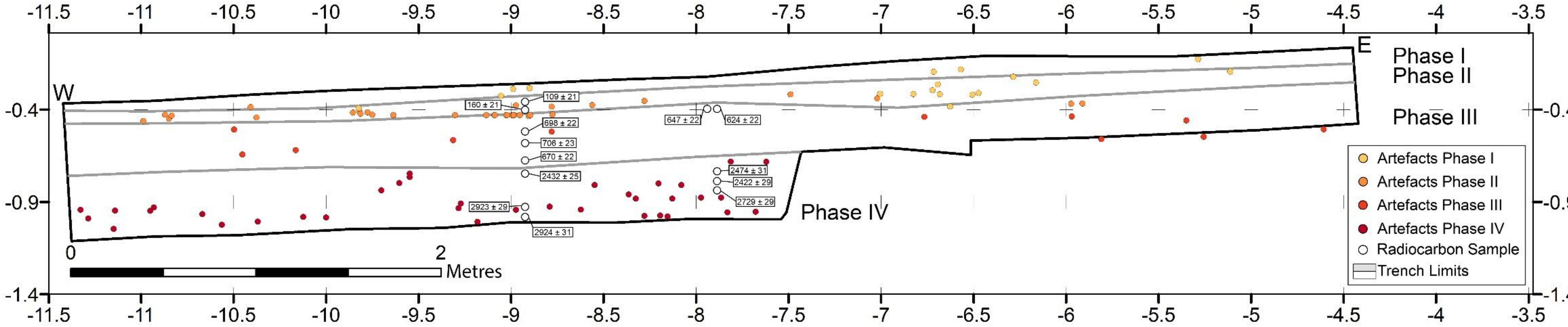

B

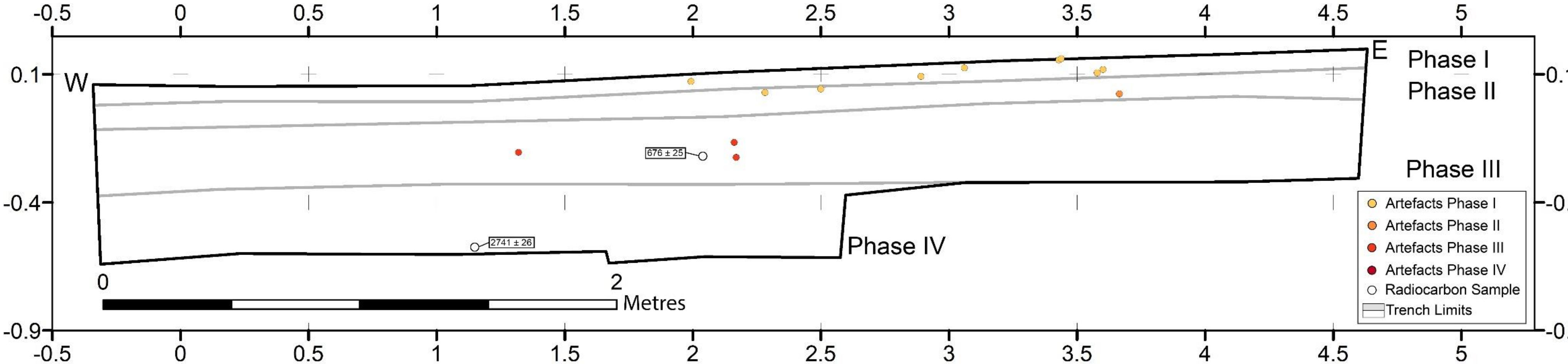

Supplementary Figure 13. *Stratigraphic position and results of all radiocarbon dates taken from Caju BPF2.* ***(A)*** *North-facing section of Caju BPF2 West.* ***(B).*** *North-facing section of Caju BPF2 East. Lines separating the Phases are guides only, because the section drawings do not fully capture the sloping nature of the site.*

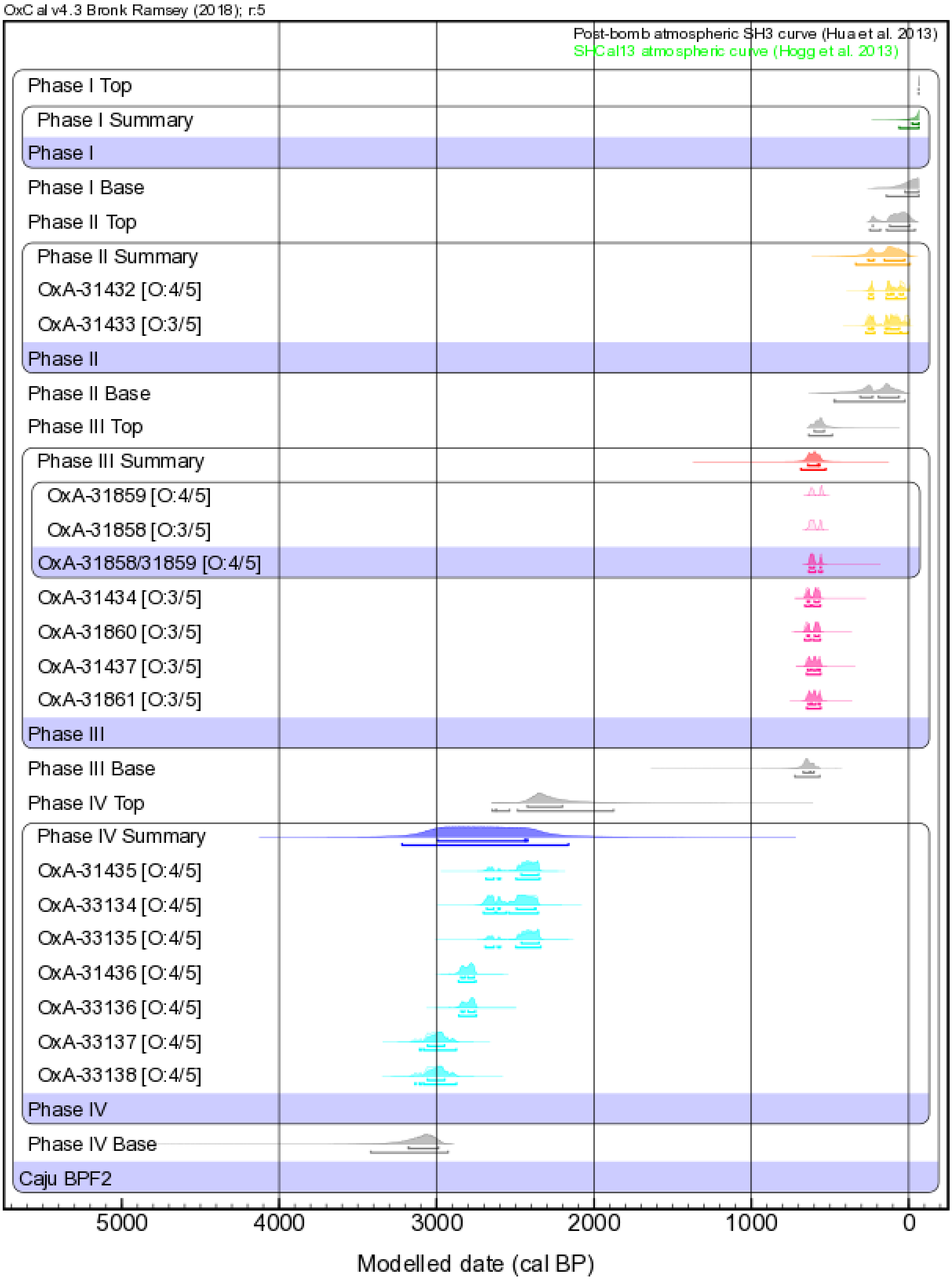

Supplementary Figure 14. Output of the Bayesian chronological modeling applied to the *radiocarbon data from Caju BPF2. Summary age distributions are provided for each of the four depositional phases associated with capuchin stone tools. (Horizontal bars below each probability distribution represent the 68.2% and 95.4% highest probability density ranges, respectively. ** Sample OxA-33133 (FUMDHAM no. 226235) provided a posterior outlier probability of 58% when* *included in a previous iteration of the Bayesian statistical model and was therefore excluded from our preferred, finalised age-depth model.*

Supplementary Table 2 **|** *Absolute and relative frequencies of technological categories identified at Caju BPF2, Serra da Capivara National Park, Brazil.*

	Stratigraphic Phase									
Secondary Technological Category	Phase I		Phase II		Phase III		Phase IV		Total	
	n	%	n	%	n	%	N	%	n	%
Anvil	2	4.3	8	34.8	3	20.0	0	0.0	13	10.7
Anvil fragment	2	4.3	6	26.1	0	0.0	0	0.0	8	6.6
Complete hammerstone	40	85.1	5	21.7	9	60.0	21	56.8	75	61.5
Hammerstone with flake detachment	1	2.1	0	0.0	1	6.7	12	32.4	14	11.5
Broken hammerstone	1	2.1	3	13.0	0	0.0	4	10.8	8	6.6
Percussive flake	1	2.1	0	0.0	1	6.7	0	0.0	2	1.6
Angular Chunk	0	0.0	1	4.3	1	6.7	0	0.0	2	1.6
Total	47	100.0	23	100.0	15	100.0	37	100.0	122	100.0

Supplementary Table 3*. Dimensions of all technological categories at Caju BPF2, separated by chronological phase.*

		Stratigraphic Phase																Total Assemblage			
		Phase I				Phase II				Phase III				Phase IV							
		Min	**Max**	**Mean**	**St.Dev**	**Min**	**Max**	**Mean**	**St.Dev**	**Min**	**Max**	**Mean**	**St.Dev**	**Min**	**Max**	**Mean**	**St.Dev**	**Min**	**Max**	**Mean**	**St.Dev**
Anvil	Max Length (mm)	89.30	111.80	100.55	15.91	84.50	216.30	161.44	49.34	146.70	204.20	178.73	29.31	-	-	-	-	84.50	216.30	156.06	47.39
	Max Width (mm)	59.90	86.40	73.15	18.74	58.80	154.40	120.81	37.85	124.40	180.30	144.07	31.42	-	-	-	-	58.80	180.30	118.85	39.23
	Max Thickness (mm)	58.40	75.00	66.70	11.74	27.20	136.00	77.40	30.78	93.20	142.00	115.00	24.81	-	-	-	-	27.20	142.00	84.43	31.40
	Weight (g)	368.50	920.00	644.25	389.97	171.40	5490.00	2280.31	1651.12	2125.80	4420.00	3408.60	1170.93	-	-	-	-	171.40	5490.00	2288.98	1611.14
Anvil Fragment	Max Length (mm)	72.00	72.60	72.30	0.42	61.90	124.20	95.80	24.65	-	-	-	-	-	-	-	-	61.90	124.20	89.93	23.50
	Max Width (mm)	32.30	52.10	42.20	14.00	40.20	95.00	63.48	22.87	-	-	-	-	-	-	-	-	32.30	95.00	58.16	22.33
	Max Thickness (mm)	16.70	18.10	17.40	0.99	11.40	46.70	29.53	14.05	-	-	-	-	-	-	-	-	11.40	46.70	26.50	13.14
	Weight (g)	39.60	66.10	52.85	18.74	31.20	592.10	204.82	206.09	-	-	-	-	-	-	-	-	31.20	592.10	166.83	187.98
Complete Hammerstone	Max Length (mm)	37.80	152.59	66.10	19.11	64.00	110.30	80.04	17.76	40.20	107.90	62.83	20.46	42.00	81.50	57.97	11.11	37.80	152.59	64.36	17.84
	Max Width (mm)	34.10	85.89	49.37	10.85	49.20	75.40	57.40	10.48	37.70	75.20	50.11	12.86	32.32	68.20	43.84	9.05	32.32	85.89	48.45	10.97
	Max Thickness (mm)	14.60	68.70	36.45	10.25	40.00	47.50	43.00	2.85	24.58	64.10	35.21	12.51	19.40	46.20	31.97	6.36	14.60	68.70	35.48	9.57
	Weight (g)	7.26	629.30	160.00	121.09	168.50	614.40	291.16	182.70	39.50	593.30	157.37	169.20	43.80	247.30	104.01	58.18	7.26	629.30	152.75	124.66
Hammerstone with flake detachment	Max Length (mm)	67.30	67.30	67.30	-	-	-	-	-	104.50	104.50	104.50	-	39.00	82.00	56.91	13.34	39.00	104.50	61.05	17.74
	Max Width (mm)	44.90	44.90	44.90	-	-	-	-	-	94.40	94.40	94.40	-	29.40	56.20	42.31	7.95	29.40	94.40	46.22	15.69
	Max Thickness (mm)	25.50	25.50	25.50	-	-	-	-	-	65.80	65.80	65.80	-	25.47	46.30	32.90	6.38	25.47	65.80	34.72	10.88
	Weight (g)	112.10	112.10	112.10	-	-	-	-	-	780.20	780.20	780.20	-	43.50	293.70	102.58	70.51	43.50	780.20	151.66	192.20
Broken Hammerstone	Max Length (mm)	58.00	58.00	58.00	-	58.90	107.30	75.97	27.17	-	-	-	-	48.30	88.50	60.01	19.08	48.30	107.30	65.74	20.95
	Max Width (mm)	43.10	43.10	43.10	-	51.20	64.50	56.57	7.01	-	-	-	-	39.20	47.30	43.93	3.67	39.20	64.50	48.56	7.99
	Max Thickness (mm)	26.40	26.40	26.40	-	21.80	55.80	36.17	17.60	-	-	-	-	31.50	41.40	36.92	4.22	21.80	55.80	35.32	10.45
	Weight (g)	74.10	74.10	74.10	-	76.70	522.70	225.57	257.33	-	-	-	-	70.10	232.20	124.83	73.17	70.10	522.70	156.26	157.48
Percussive Flake	Max Length (mm)	75.40	75.40	75.40	-	-	-	-	-	43.40	43.40	43.40	-	-	-	-	-	43.40	75.40	59.40	22.63
	Max Width (mm)	39.10	39.10	39.10	-	-	-	-	-	32.30	32.30	32.30	-	-	-	-	-	32.30	39.10	35.70	4.81
	Max Thickness (mm)	14.10	14.10	14.10	-	-	-	-	-	8.70	8.70	8.70	-	-	-	-	-	8.70	14.10	11.40	3.82
	Weight (g)	35.70	35.70	35.70	-	-	-	-	-	12.20	12.20	12.20	-	-	-	-	-	12.20	35.70	23.95	16.62
Angular Chunk	Max Length (mm)	-	-	-	-	92.20	92.20	92.20	-	102.50	102.50	102.50	-	-	-	-	-	92.20	102.50	97.35	7.28
	Max Width (mm)	-	-	-	-	40.60	40.60	40.60	-	77.20	77.20	77.20	-	-	-	-	-	40.60	77.20	58.90	25.88
	Max Thickness (mm)	-	-	-	-	32.20	32.20	32.20	-	72.00	72.00	72.00	-	-	-	-	-	32.20	72.00	52.10	28.14
	Weight (g)	-	-	-	-	123.60	123.60	123.60	-	584.90	584.90	584.90	-	-	-	-	-	123.60	584.90	354.25	326.19

Context	Sample Ref. (FUMDHAM no.)	Dept h (cm)	Sub-sample wt. (mg)	Combustion Yield (% C)	ORAU Lab. no. (OxA-)	Conventional ^{14}C Age ± 1□	□^{13}C (‰)	Modeled Age (68.2% and 95.4% highest probability density ranges cal BP)		Posterior Outlier Probability (%)
Phase I								**-23 to -64 (1973 to 2014 cal AD)**	**60 to -64 (1890 to 2014 cal AD)**	
Phase II								**257 to 27 (1693 to 1924 cal AD)**	**336 to -8 (1614 to 1958 cal AD)**	
G02,L03	221879	7.9	84.6	52.9	31432	109 ± 21	-26.3	249 to 35	255 to 19	4
G02,L04	221916	12.3	91.1	56.8	31433	160 ± 21	-26.0	256 to 59	271 to 4	3
Phase III								**640 to 565 (1310 to 1385 cal AD)**	**685 to 527 (1265 to 1423 cal AD)**	
G03,L05	221934 *	16.5	81.6	69.1	31858	647 ± 22	-23.2	629 to 558	635 to 550	3
G03,L05	221934 *	16.5	72.4	62.6	31859	624 ± 22	-23.7	629 to 558	635 to 550	4
G02,L06	221947	21.0	125.0	63.0	31434	698 ± 22	-23.5	644 to 568	658 to 561	3
G02,L07	221963	26.0	92.2	70.2	31860	706 ± 23	-23.7	645 to 569	661 to 562	3
G13,L07	221526	31.1	138.8	60.3	31437	676 ± 25	-26.6	643 to 563	649 to 560	3
G02,L09	221974	34.6	73.4	65.9	31861	670 ± 22	-23.4	639 to 562	648 to 559	4
Phase IV								**2993 to 2422 (1044 to 473 cal BC)**	**3218 to 2163 (1269 to 214 cal BC)**	
G02,L10	221988	39.3	104.0	57.0	31435	2432 ± 25	-25.8	2463 to 2353	2687 to 2345	4
D03,L10	226235	52.0	108.3	65.2	33133	3698 ± 33	-23.4	4076 to 3908	4090 to 3867	**
D03,L11	226259	57.0	88.9	59.8	33134	2474 ± 31	-24.7	2683 to 2371	2703 to 2355	4
D03,L12	226293	63.0	77.0	62.3	33135	2422 ± 29	-26.0	2462 to 2350	2691 to 2339	4
G12,L14	219514	63.2	159.4	56.3	31436	2741 ± 26	-25.4	2843 to 2760	2859 to 2752	4
D03,L13	226368	68.0	76.2	60.6	33136	2729 ± 29	-26.0	2842 to 2754	2857 to 2748	4
D02,L15	226404	73.0	36.8	60.1	33137	2923 ± 29	-25.6	3056 to 2949	3107 to 2873	4
D02,L16	226486	77.0	106.8	66.9	33138	2924 ± 31	-22.9	3057 to 2947	3136 to 2872	4

Supplementary Table. 1. *Radiocarbon ages of charcoal samples from Caju BPF2, Serra da Capivara National Park, Brazil. Modeled Age is given at 68.2% and 95.4% ranges, which are approximations for the 1-sigma and 2-sigma ranges of Normally-distributed data, respectively. Age ranges are given in calibrated years before present (cal.BP), except for the parentheses associated with the depositional unit summary data where values are given in 'cal.AD/BC'.*

* Two sub-samples of duplicated sample FUMDHAM no. 221934

** Sample OxA-33133 (FUMDHAM no. 226235) provided a posterior outlier probability of 58% when included in a previous iteration of the Bayesian statistical model and was therefore excluded from our preferred, finalised age-depth model.

Bibliography

1. Wentworth, C. K. A laboratory and field study of cobble abrasion. J. Geol. 27, 507–521. (1919).

2. Sneed, E. D. & Folk, R. L. Pebbles in the lower Colorado River, Texas a study in particle morphogenesis. J. Geol. 66, 114–150 (1958).

3. Brock, F., Higham, T., Ditchfield, P., and Bronk Ramsey, C. (2010). Current pretreatment methods for AMS radiocarbon dating at the Oxford Radiocarbon Accelerator Unit (ORAU). Radiocarbon 52, 103-112.

4. Bronk Ramsey, C., Higham, T., and Leach, P. (2004). Towards high-precision AMS: progress and limitations. *Radiocarbon* 46, 17-24.

5. Staff, R.A., Reynard, L., Brock, F., and Ramsey, C.B. (2014). Wood pretreatment protocols and measurement of tree-ring standards at the Oxford Radiocarbon Accelerator Unit (ORAU). Radiocarbon 56, 709-715.

6. Bronk Ramsey, C. (2018) OxCal ver.4.3, https://c14.arch.ox.ac.uk/oxcal/OxCal.html.

7. Hogg, A., Hua, Q., Blackwell, P., Niu, M., Buck, C., Guilderson, T., and Zimmerman, S. (2013). SHCal13 Southern Hemisphere Calibration, 0-50,000 Years cal BP. Radiocarbon 55.

8. Hua, Q., Barbetti, M., and Rakowski, A.Z. (2013). Atmospheric radiocarbon for the period 1950–2010. Radiocarbon 55, 2059-2072.

9. Bronk Ramsey, C. (1995). Radiocarbon calibration and analysis of stratigraphy; the OxCal program. Radiocarbon 37, 425-430.

10. Bronk Ramsey, C. (2008). Deposition models for chronological records. Quat. Sci. Rev. 27, 42-60.

11. Macken, A.C., Staff, R.A., and Reed, E.H. (2013). Bayesian age-depth modelling of Late Quaternary deposits from Wet and Blanche Caves, Naracoorte, South Australia: A framework for comparative faunal analyses. Quat. Geochronol. 17, 26-43.

12. Bronk Ramsey, C. (2009). Dealing with outliers and offsets in radiocarbon dating. Radiocarbon 51, 1023-1045.